Nanoscale

Accepted Manuscript

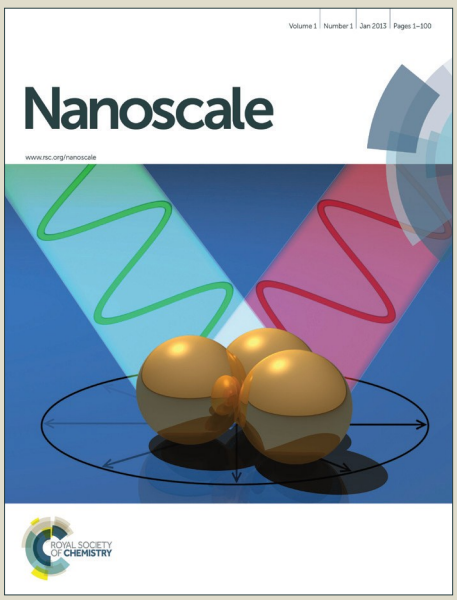

ROYAL SOCIETY OF CHEMISTRY

www.rsc.org/nanoscale

Journal Name

ARTICLE TYPE

Cite this: DOI: 10.1039/xxxxxxxxxx

Growth of single-layer boron nitride dome-shaped nanostructures catalysed by iron clusters†

A. La Torre,[*a,b] E. H. Åhlgren,[b] M. W. Fay,[c] F. Ben Romdhane,[a] S. T. Skowron,[b] C. Parmenter,[b] A. J. Davies,[c] J. Jouhannaud,[a] G. Pourroy,[a] A. N. Khlobystov,[b,c] P. D. Brown[c,d] E. Besley[*b] and F. Banhart[*a]

Received Date
Accepted Date

DOI: 10.1039/xxxxxxxxxx

www.rsc.org/journalname

We report on the growth and formation of single-layer boron nitride dome-shaped nanostructures mediated by small iron clusters located on flakes of hexagonal boron nitride. The nanostructures were synthesized in situ at high temperature inside a transmission electron microscope while the e-beam was blanked. The formation process, typically originating at defective step-edges on the boron nitride support, was investigated using a combination of transmission electron microscopy, electron energy loss spectroscopy and computational modelling. Computational modelling showed that the domes exhibit a nanotube-like structure with flat circular caps and that their stability was comparable to that of a single boron nitride layer.

1 Introduction

Graphitic sheets of carbon can form various architectures, such as nanotubes, fullerenes or carbon "onions"[1–9]. In this context, an interesting new class of carbon nanostructure has been reported, termed "nanobud" or "protrusion", emerging directly from planar graphene or carbon nanotubes [10–12]. Such "dome-like" features exhibit positive as well as negative curvature, requiring both pentagonal and heptagonal structural units, and have the potential to act as starting points for nanotube growth[13–15].

In principle, such architectures should be achievable also within single layer boron nitride (BN), on flat or tubular sp2-hybridized BN supports, but the realization of such structures also requires the arrangement of non-hexagonal rings, and this creates an important restriction for BN materials, because structures with odd-membered rings (pentagons, heptagons) require energetically unfavourable B-B or N-N bonds. Nevertheless, the existence of even membered rings in BN containing B-B and N-N bonds has been demonstrated[16] and through the introduction of quadrilateral or octagonal rings to the hexagonal network, BN topologies with either positive or negative curvature, become feasible[17–22]. Appropriate synthetic approaches to control the assembly of non-planar BN nanostructures, in terms of size, shape and local composition, are now required.

Here, we report on an *in situ* transmission electron microscopy (TEM) investigation, at elevated temperature, demonstrating for the first time that single layer BN dome-shaped nanostructures can be formed directly on planar BN supports via the catalytic action of metal clusters. It is considered, that the growth of BN nanostructures arises originating from defective step-edges on the BN support. We use molecular dynamics simulations to elucidate the atomic structure and thermodynamic stability of these nanostructures, and present TEM image simulations using the calculated structures to show excellent agreement with experimental images of these features observed at various angles relative to the incident electron beam.

2 Experiment

A suspension of few layer BN (FLBN) aggregates was drop cast onto a gold mesh TEM grid and heated to 550°C in a tube furnace

[a] Institut de Physique et Chimie des Matériaux de Strasbourg, UMR 7504 CNRS, Université de Strasbourg, 23 rue du Loess, 67034 Strasbourg, France. E-mail: alessandro.latorre@nottingham.ac.uk, florian.banhart@ipcms.unistra.fr
[b] School of Chemistry, University of Nottingham, University Park, Nottingham, NG7 2RD, UK. Email: elena.besley@nottingham.ac.uk
[c] Nanoscale and Microscale Research Centre, University of Nottingham, University Park, Nottingham, NG7 2RD, UK.
[d] Department of Mechanical, Materials and Manufacturing Engineering, Faculty of Engineering, University of Nottingham, University Park, Nottingham, NG7 2RD, UK.

† Electronic Supplementary Information (ESI) available. See DOI: 10.1039/b000000x/

in air, to remove adventitious carbon. By Raman spectroscopy the FLBN flakes were found to exhibit a single band at 1363 cm^{-1}, characteristic of the hexagonal BN (*h*-BN) phase[23] (Figure S1†). A few drops of methanolic suspension containing Fe_2O_3 nanoparticles (NP), 11.2 ± 0.5 nm in diameter, were cast onto these freshly annealed FLBN supports and then heated in vacuum at 750°C for 30 minutes within the heating specimen stage of the TEM, with the electron beam blanked in order to avoid any electron beam-induced transformations, see Figure 1.

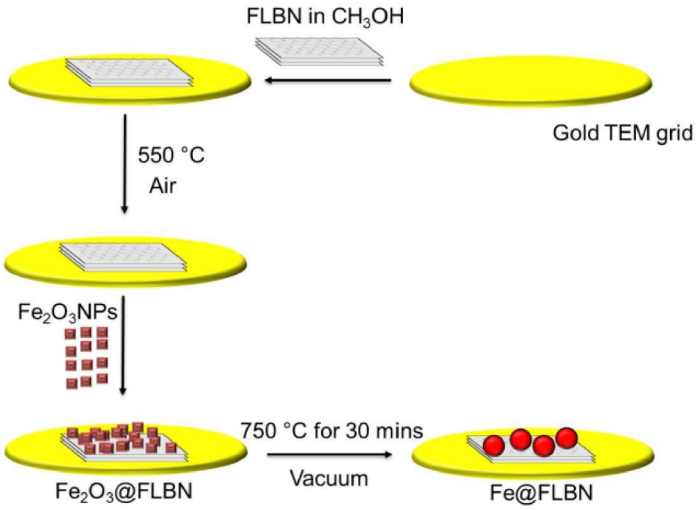

Fig. 1 Processing of composite Fe_2O_3@FLBN on a gold TEM support grid to form Fe at@FLBN.

During the heating process, the Fe_2O_3 NPs (Figure 2(a)) reduced to form pure, small metallic Fe clusters, which then ripened to form Fe NPs, about 30 nm in diameter (Figure 2(b)), with the BN support acting as a reducing agent, *i.e.* $Fe_2O_3 + 2BN \rightarrow 2Fe + B_2O_3^{\uparrow} + N_2^{\uparrow}$. Upon reduction, the Fe_2O_3 NPs effectively etched the FLBN surface, creating step-edges with open bonds, see Figures 2(b) and 3(a). Electron energy loss spectroscopy (EELS) (Figures 2(c,d)) confirmed the transformation of Fe_2O_3 to pure Fe, as the oxygen edge is seen to vanish after reduction. Typical B and N edges are present at 188 eV and 401 eV, respectively, consistent with the presence of *h*-BN.

Subsequent heating of the sample at 750°C for a further 60 minutes, with the electron beam blanked, showed that the step-edges on the BN flakes acted as anchoring points for the Fe clusters. These small iron clusters were released from the big iron particles. The BN dome-like nanostructures began developing during the annealing process and in some cases were still decorated with residual few-atom Fe clusters (Figure 3(a) arrowed). The lack of a carbon peak at 284 eV in the corresponding EEL spectra confirmed that the structures were not graphitic.

Extended heating at 750°C for 120 minutes led to the formation of more well-defined, single-layer BN protrusions of 3.2 nm average diameter, again residing at the step-edges of the FLBN support (Figure 4). In some cases, the nanostructures exhibited faceted topologies (Figures 4(b,c)) and in few instances Fe metal clusters remained inside.

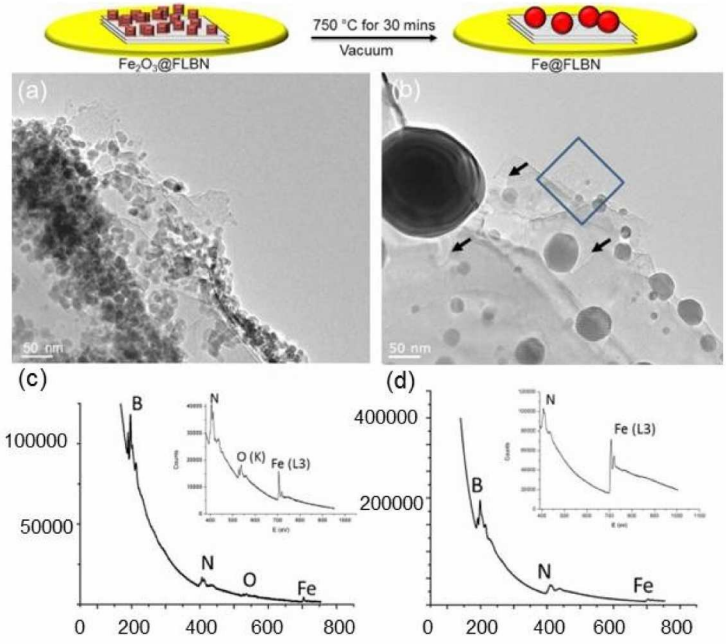

Fig. 2 (a,b) Bright field TEM images and (c,d) EEL spectra of FLBN flakes decorated with (a,c) synthesized Fe_2O_3 NP; and (b,d) reduced Fe NP after heating in situ at 750°C in vacuum for 30 minutes. (b) Arrows denote the etched areas where the BN support layer has disappeared. The blue rectangle denotes the area shown in Figure 3.

3 Computational simulations

Complementary molecular dynamic (MD) simulations showed the viability of stable, dome-shaped BN features protruding from a single BN layer, exhibiting nanotube-like structures with flat circular caps (Figure 5(a)). Such BN caps have been shown, both experimentally and theoretically[17–21], to have sharp edges and corners, thus requiring the presence of topological defects in the hexagonal structure, such as four-membered rings located at the cap corners. BN nanotubes, for example, can be closed by flat caps via the incorporation of four- and eight-membered rings into the structure[17], being distinct from caps associated with the closure of carbon nanotubes, which resemble fullerene-like hemispheres consisting of pentagons and hexagons[14].

The thermodynamically stable *h*-BN dome structure presented in Figure 5(a) was obtained from MD simulation upon initial heating to 600 K followed by stepwise cooling down to 0 K. The resultant nanostructure exhibits a number of residual defects, *i.e.* non-hexagonal rings aligned along the interfaces between the *h*-

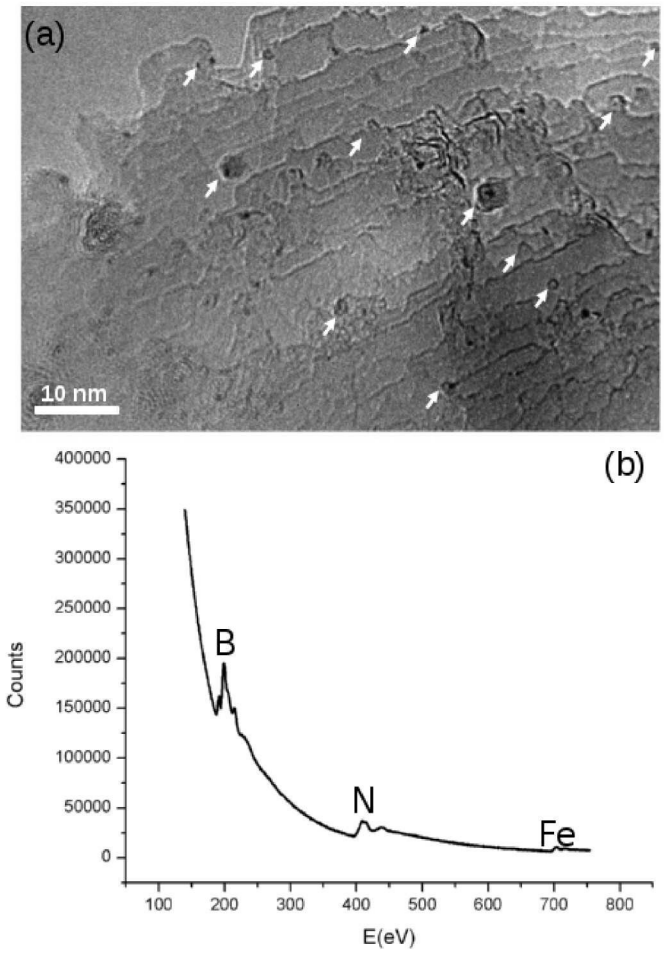

Fig. 3 (a) Bright field TEM image showing step edges on FLBN - image acquired at 750°C, after 60 minutes of in situ heating in vacuum; and (b) corresponding EEL spectrum consistent with the presence of pure *h*-BN. Arrows denote BN protrusions, some of which were decorated with few-atom Fe clusters.

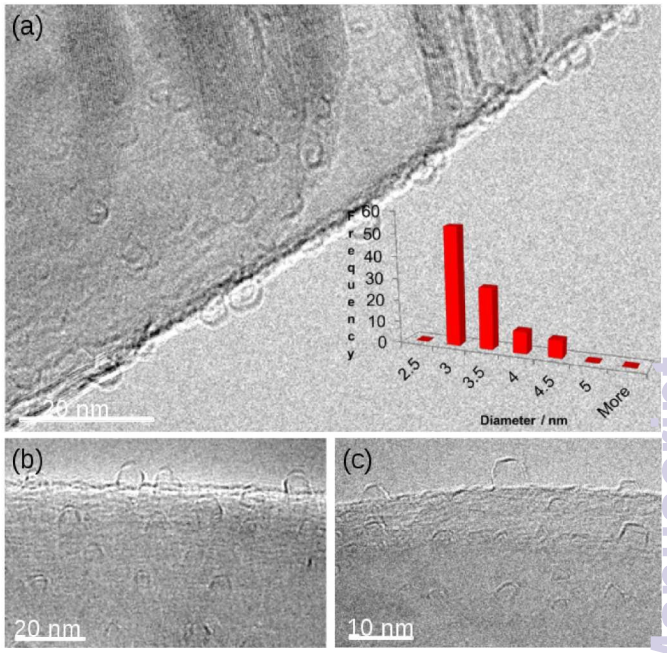

Fig. 4 (a-c) Bright field TEM images of single layer BN dome-like structures, formed after *in situ* heating at 750°C for 120 minutes (feature size histogram inset: 2.6 - 4.4 nm).

BN layer and the wall of the dome, as well as the cap and the wall, and contains no dangling bonds. A small number of defects are required to allow for full closure of the nanostructure. A histogram of the defect distribution corresponding to the dome structure shown in Figure 5(a) is presented in Figure 5(b); noting that the position of defect types at the interfaces varies with local curvature. The exact defect structure is shown in the supplement, Figure S3[†]. The total energy of the *h*-BN dome shown in Figure 5(a) after full relaxation of its structure at 0 K is −12.77 eV per B-N pair, which is only 0.06 eV per B-N pair higher than the energy of a perfect single *h*-BN layer, indicating good thermodynamic stability. Furthermore, the *h*-BN nanostructure obtained is significantly more stable than a typical closed BN cage.

Haishun *et al.*[24] used density functional theory to show that small BN cages obey a simple topological rule to describe the number of bonds between four-membered rings (squares). Energetically unfavourable structures contain a large number of adjacent squares with no bonds in between (this connection is denoted as 404-type), whilst increasing the number of bonds between squares leads to a decrease in the energy penalty. To illustrate this, BN cages of three different sizes, *i.e.* $(BN)_{12}$, $(BN)_{15}$ and $(BN)_{18}$, were considered in order to appraise the effect of four-membered rings in the BN structure on its stability. The candidate structures have the same number of four-membered rings but differ in number of bonds connecting them. The corresponding total energies, per B-N pair, after heating to 600 K and stepwise cooling to 0 K (step size 50 K) are presented in Table 5(c). The smallest $(BN)_{12}$ cage is found to be most energetically unfavourable, having eight 414-type connections and the total energy of −9.83 eV per B-N pair. For larger $(BN)_{15}$ and $(BN)_{18}$ cages, the energy per B-N pair is lower by 0.45 eV and 0.79 eV, respectively, due to a reduction in the number of 414-type bonds. Further comparison of $(BN)_{15}$ and $(BN)_{18}$ cages enables the effect of 424-type connections on the stability of BN structures to be appraised. The $(BN)_{15}$ cage, having six 424-type connections, resulted in a higher total energy, by 0.34 eV per B-N pair, as compared to the $(BN)_{18}$ cage with no 424-type connections in its structure. This indicates that the energetic cost of 414-type bonding is higher than the cost of 424-type bonding, in agreement with Haishun *et al.*[24]. The large single layer *h*-BN dome-like structure

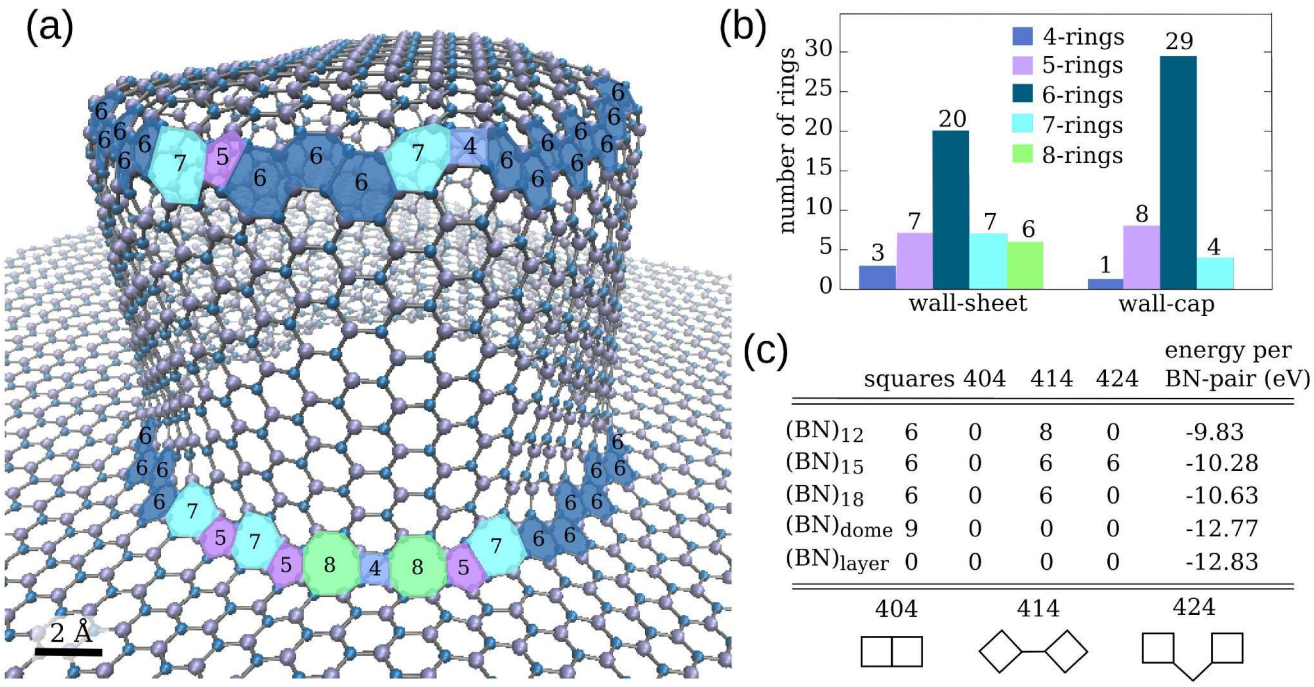

Fig. 5 An example of a stable *h*-BN dome protruding from an *h*-BN sheet, as predicted by molecular dynamics simulations, showing: (a) pictorial distribution of defects at the layer and cap interfaces; (b) histograms of the corresponding atomic rings; and (c) values of total energy (per B-N pair), the number of four-membered rings in the nanostructure, and three main types of connections between the squares in $(BN)_{12}$, $(BN)_{15}$ and $(BN)_{18}$ cages, (BN) dome and a perfect single *h*-BN layer.

shown in Figure 5(a) involves five four-membered rings spatially well separated, but no 404-, 414- or 424-type connections, leading to a significantly more stable structure, by about 2 eV per B-N pair, than a typical closed BN cage.

TEM image simulations of this calculated nanostructure were produced using QSTEM multi-slice code[25] with simulation parameters selected to match the experimental imaging conditions (see Computational Details-section). With respect to the proposed growth mechanism, it is considered that these nano-buds form preferentially at FLBN step-edges and protrude from the *h*-BN plane at an angle. The *h*-BN dome-shaped nanostructure of Figure 5 (a) was used to simulate images of BN protrusions at various angles relative to the incident electron beam, by adjusting effectively the beam direction. Figures 6 (a-d) present simulated images for beam angles of 0°, 30° and 50°, respectively, relative to the *h*-BN plane normal, in comparison with experimentally observed features (Figures 6 (e-h)). The image simulations are in striking agreement with the experimental images, consistent with the circular features being protrusions formed normal to the *h*-BN plane, whilst the hemispheres correspond to protrusions tilted with respect to the *h*-BN plane.

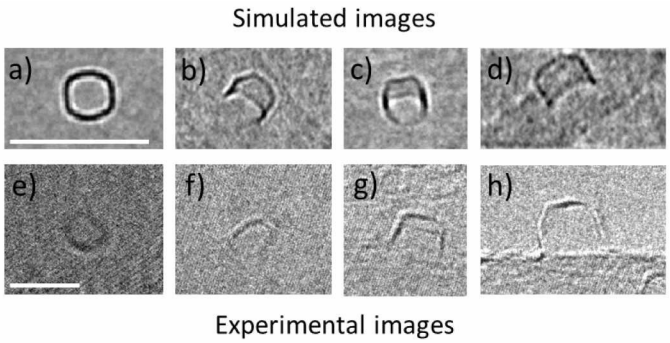

Fig. 6 Simulated TEM images (a-d) of the *h*-BN dome-like nanostructure presented in Figure 5 corresponding to incident beam directions of (a) 0°, (b-c) 30° and (d) 50° with respect to the *h*-BN plane; (e-h) Experimentally observed features (from Figure 4 and Figure S2†) for comparison with the simulations. The scale bars are 10 nm, and are shown in the first image of each row for the whole row.

4 Results and discussion

The cutting and restructuring of layers of graphene by mobile transition metal nanoparticles at high temperature is a well-known process[26,27], and the extrusion of graphitic carbon from transition metals has been reported in the context of growth of carbon nanotubes and graphene[26]. A related effect is described

here for boron nitride, with Figure 3 providing evidence for the catalytic etching of the *h*-BN support layers in advance of the formation of dome-shaped BN nanostructures. It is considered that the B_2O_3 and N_2 reaction products evaporate[28] during processing, as the Fe_2O_3 NP reduce to Fe NP. Under conditions of atmospheric pressure B_2O_3 evaporates at 1500°C, and hence is likely to sublime at 750°C under the conditions of high vacuum in the TEM.

In the present study, it is considered that Fe atom clusters originating from the large Fe NP's (>30 nm) diffuse and become trapped along the dangling bonds and defect sites of BN sheet step-edges.

Two different mechanisms could then explain the formation of the protrusions. One possibility is the dissolution-precipitation mechanism, whereby BN dissociates on the surface of the Fe clusters (noting B and N atoms are soluble in iron)[29–31], followed by dissolution, diffusion and precipitation of BN in a form of dome-shaped nanostructures (diameter 2.6 - 4.4 nm) in advance of loss of the Fe at elevated temperature. This is similar to the case of carbon nanostructures, where the nucleation of protrusions on the surfaces of metal atom clusters can occur[12]. The second possibility is the "scooter" mechanism, as proposed to explain the growth of carbon nanotubes[7]. Here, mobile Fe atoms could continue to etch the BN layers in such a way that small strips remain that subsequently curl and close to form dome-shaped nanostructures. After nanostructure closure, the Fe atoms may either remain trapped inside the cage or escape, depending on the heating conditions or on the experimental conditions. However, in this instance, the growth mechanism can be solely speculated, as the fabrication of the half-dome structures occur while the e-beam was blanked, and not under e-beam irradiation as it has been previously reported for BN fullerene like-species[21].

Nanostructured carbon protrusions have been studied since 2001[7,11,12], but the investigation of analogous BN structures has only just begun. In the present study, we have shown that even member rings are required for the formation of *h*-BN dome-shaped protrusions, but not in the form of active linear defects, containing B-B and N-N bonds, as observed recently in BN monolayers under electron beam irradiation[16]. Furthermore, according to our molecular simulation results, the even- and odd-members rings present in the half dome structure can present B-B and N-N bonds. The exact bond structure of the simulated dome is shown in the supplement, Figure S3[†]. The aligned defects at the top and the bottom of the dome bare resemblance to grain boudaries seen in planar *h*-BN[32,33], and indeed are grain boundaries between the crystalline domains of the dome.

Small transition metal clusters appear to play an important role in nanostructuring of BN. Few-atom metal clusters within *h*-BN dome-shaped nanostructures represent a new hybrid material that may unveil new optical, magnetic, electronic or catalytic properties, emerging from confinement effects. The presented synthesis could be also further developed to produce other unique BN architectures suitable for electronic devices, magnetic recording media and biological sensors with protection againts wear and oxidation. Since *h*-BN is an insulator, in contrast to graphene, charged species could be localised within the domes and lead to interesting optical phenomena. However, further studies are needed to demonstrate the controlled retention of metal clusters within dome-shaped nanostructures, through limitation of the metal extrusion process. As predicted recently, the adsorption of transition metal atom chains to the octagonal rings of protrusions may also promote promising electronic or magnetic properties, *e.g.* Cr and Ni decorated protrusions can become quasi-spin-gapless semiconductors, whilst Fe- or Co-doping induces ferromagnetic semiconductor behaviour, and Mn transforms such protrusions into antiferromagnetic semiconductors[34]. On the other hand, as the demand of clean energy has triggered an interest in the use of hydrogen in zero-emission vehicles, BN nanotubes have been shown to have promise as a hydrogen storage medium[35]. In contrast to carbon nanotubes, *h*-BN nanotubes have several attributes that indicate better stability for hydrogen storage, such as their semiconducting nature with a little effect of the tube diameter and helicity to the band gap[36]. Z. Zhou et al.[37] suggested that rather than perfect *h*-BN nanotubes, *h*-BN nanotubes as supporting media for hydrogen-absorbing metal nanoclusters might increase the storage capacity. Systems, where metal clusters are confined within BN dome-shaped nanostructures, might present such a platform.

5 Conclusions

We show that a new form of single layer boron nitride dome shaped nanostructures can be grown via a mechanism similar to the growth of nanostructured carbon protrusions, catalysed by iron nanoclusters. However, the morphologies of these BN nanostructures are distinct from their carbon analogues, requiring squares, pentagons, hexagons, heptagons and octagonal rings in their formation. On the contrary to the carbon protrusion, the BN-protrusions display sharp corners and edges. Molecular dynamics simulations confirm the stability of the BN-protrusions. The total energy per BN-pair in a 3 nm diameter protrusion is about 2 eV lower than that of a typical closed BN cage, and about 0.06 eV higher than that of a perfect single layer of *h*-BN. TEM image simulations of the BN dome-shaped structures modelled with MD show striking agreement with the experimental images. Circular features correspond to domes formed normal to the *h*-BN plane, whilst hemispheres correspond to titled structures formed at the step edges of the *h*-BN support.

6 Experimental Methods

The TEM data sets were acquired using a JEOL 2100F (point resolution 0.19 nm; accelerating voltage 200 kV) with aberration-corrected probe and Gatan imaging filter (GIF) for electron energy loss spectroscopy (EELS) at the Institut de Physique et Chimie des Matériaux de Strasbourg, France; and a JEOL 2100F (point resolution 0.19 nm; accelerating voltage 200 kV) equipped with a Gatan Tridiem imaging filter for EELS at the Nanoscale and Microscale Research Centre, University of Nottingham, U.K. A Gatan 652 double-tilt heating holder was used for the in situ TEM heating experiments. The SEM data sets were acquired using an FEI Quanta 200 3D at an accelerating voltage of 5-10 kV and working distance of 15 mm, using secondary imaging mode, at the Nanoscale and Microscale Research Centre in Nottingham; and a Jeol 6700F at the Institut de Physique et Chimie des Matériaux de Strasbourg.

Nanoparticles of iron oxide were produced using the following standard procedure. 10 mL of 1 M $FeCl_3$ solution was mixed with 2.5 mL of 2 M $FeCl_2$ solution in a flask. The mixture was heated to 70°C under Ar, with mechanical stirring, and then 21 mL of 25% $N(CH_3)_4OH$ aqueous solution was dropwise cast into the mixture. The resulting Fe_2O_3 nanoparticles (Figure S4[†]), with associated particle size histogram measured by SEM were isolated using a permanent magnet, allowing the supernatant to be decanted. Degassed water was then added to wash the precipitates. This procedure was repeated four times to remove excess ions and the tetramethylammonium salt from the suspension. The remaining precipitate was freeze dried to create a powder.

TEM supports were prepared by drop-casting a commercially available methanolic suspension of FLBN (Graphene Supermarket; lateral size of 50-200 nm and thickness of 1-5 monolayers) onto a gold mesh TEM grid and heating in air at 550°C in a tube furnace to remove adventitious carbon. The Fe_2O_3 NP were suspended in methanol and dropped on to the BN flake / gold mesh grids.

Complementary Raman spectra were acquired using a Horiba-Jobin-Yvon LabRAM Raman microscope, with a 532 nm wavelength laser operating at low power (ca. 4 mW), a 600 lines/mm grating and a Synapse CCD detector. Spectra were collected by recording four acquisitions of 1 s duration for each spectral window. The Raman shift was calibrated using the Raleigh peak and the 520.7 cm^{-1} line from a Si(100) reference sample.

7 Computational Details

Classical MD simulations were run with PARCAS code[38]. The interactions between the B and N atoms were modelled with the analytical potential by Albe and Möller[39], a Tersoff-like many-body potential fitted to a wide range of ab initio data, and in which the energy of pure B-N bonds and the structures of BN polymorphs and clusters were appraised. Lowest energy configurations were established for each structure studied by heating to 600 K for 1 ns, followed by simulation using a microcanonical NVE ensemble for 1 ns, then gradually dropping the temperature in steps of 50 K and 1 ns, with each step followed by simulation using an NVE ensemble for 1 ns, until the final temperature of 0 K was reached. For perfect *h*-BN sheets and protrusions, periodic boundary conditions in the x- and y-directions were utilised, with the perfect sheets being 10 × 10 nm in size, including 3854 atoms.

TEM image simulations were produced using the QSTEM multislice code[25]: accelerating voltage = 200 kV, Cs = 0.1 mm, defocus = -65 nm, resolution = 1 Å/pixel. The noise due to the finite electron dose was then applied, with the intensity of each pixel calculated as:

$$I(x,y) = Poisson\ random[I_{sim}(x,y)D\Delta x\Delta y], \quad (1)$$

where $I_{sim}(x,y)$ is the image intensity resulting from multislice simulation, D is the electron dose per image (about 10^4 e^-/nm^2) and $\Delta x\Delta y$ is the pixel size. A simulated modulation transfer function of the CCD camera at 200 kV was then applied to obtain an accurate signal to noise ratio[40].

8 Acknowledgements

A.L.T. and E.H.Å thank Dr Matteo Baldoni for discussion. The authors acknowledge the support of the TEM facilities at the University of Strasbourg and the Nanoscale and Microscale Research Centre (NMRC) at Nottingham. A.L.T thanks the Natural Environment Research Council (NERC) for supporting this work. E.B. acknowledges an ERC Consolidator grant.

9 Abbreviations

FLBN few layer boron nitride; NP nanoparticles; *h*-BN hexagonal boron nitride; EELS electron energy loss spectroscopy; TEM transmission electron microscopy; SEM scanning electron microscopy; MD molecular dynamics.

References

1 H. Terrones, M. Terrones, E. Hernandez, N. Grobert, J. C. Charlier and P. M. Ajayan, *Phys. Rev. Lett.*, 2000, **84**, 1716–1719.
2 M. Endo, H. Muramatsu, T. Hayashi, Y. A. Kim, M. Terrones and M. S. Dresselhaus, *Nature*, 2005, **433**, 476.
3 S. Iijama and T. Ichihashi, *Nature*, 1993, **363**, 603–605.
4 A. Chuvilin, U. Kaiser, E. Bichoutskaia, N. A. Besley and A. N. Khlobystov, *Nature Chemistry*, 2010, **2**, 450–453.
5 N. S. Goroff, *Acc.Chem. Res.*, 1996, **29**, 77–83.
6 H. W. Kroto and K. McKay, *Nature*, 1988, **331**, 328–331.
7 R. Sharma, P. Rez, M. M. J. Treacy and S. J. Stuart, *J. Electron Micros.*, 2005, **54**, 231–237.

8 M. S. Zwanger, F. Banhart and A. Seeger, *J. Cryst. Growth*, 1996, **163**, 445–454.

9 F. Banhart and P. M. Ajayan, *Nature*, 1996, **382**, 433–435.

10 Y. Zhao, Y. Lin and B. I. Yakobson, *Phys. Rev. B*, 2003, **68**, 233403.

11 T. W. Chamberlain, J. C. Meyer, J. J. Biskupek, J. Leschner, A. Santana, N. A. Besley, E. Bischoutskaia, U. Kaiser and A. N. Khlobystov, *Nature Chemistry*, 2011, **3**, 732–737.

12 A. G. Nasibulin, P. V. Pikhitsa, H. Jiang, D. P. Brown, A. V. Krasheninnikov, A. S. Anisimov, P. Queipo, A. Moisala, D. Gonzalez, G. Lientschnig, A. Hassanien, S. D. Shandakov, G. Lolli, D. E. Resasco, M. Choi, D. Tomanek and E. I. Kauppinen, *Nature Nanotech.*, 2007, **2**, 156–161.

13 J. Gavillet, A. Loiseau, C. Journet, F. Willaime, F. Ducastelle and J.-C. Charlier, *Phys. Rev. Lett.*, 2001, **87**, 275504.

14 S. Reich, L. Li and J. Robertson, *Phys. Rev. B*, 2005, **72**, 165423.

15 R. S. Lee, J. Gavillet, M. L. de la Chapelle, A. Loiseau, J.-L. Cochon, D. Pigache, J. Thibault and F. Willaime, *Phys. Rev. B*, 2001, **64**, 121405.

16 O. Cretu, Y. C. Lin and K. Suenaga, *Nano Lett.*, 2014, **14**, 1064–1068.

17 O. Stephan, Y. Bando, A. Loiseau, F. Willaime, N. Shramchenko, T. Tamiya and T. Sato, *Appl. Phys. A Mat. Sci. Proc*, 1998, **67**, 107–111.

18 T. Oku, T. Hirano, M. Kuno, T. Kusunose, K. Niihara and K. Suganuma, *Mat. Sci and Engin.*, 2000, **B74**, 206–217.

19 M. Terrones, W. K. Shu, H. Terrones, J. P. Zhang, S. Ramos, J. P. Hare, R. Castillo, K. Prassides, A. K. Cheetham, H. W. Kroto and D. R. M. Walton, *Chem. Phys. Lett.*, 1996, **259**, 568–573.

20 N. G. Chopra, R. J. Luyken, K. Cherrey, V. H. Crespi, M. L. Cohen, S. G. Louie and A. Zettl, *Science*, 1995, **269**, 966–967.

21 D. Golberg, Y. Bando, Y. Huang, T. Terao, M. Mitome, C. Tang and C. Zhi, *ACS Nano*, 2010, **4**, 2979–2993.

22 F. Banhart, M. Zwanger and H.-J. Muhr, *Chem. Phys. Lett.*, 1994, **231**, 98–104.

23 S. Reich, A. C. Ferrari, R. Arenal, A. Loiseau, I. Bello and J. Robertson, *Phys. Rev. B*, 2005, **71**, 205201.

24 W. Haishun and T. Xinxin, *CJI*, 2006, **8**, 29.

25 C. Koch, *Determination of core structure periodicity and point defect density along dislocations*, PhD Thesis, Arizona State University, 2002.

26 J. A. Rodriguez-Manzo, C. Pham-Huu and F. Banhart, *ACS Nano*, 2011, **2**, 1529–1534.

27 G. Melinte, I. Florea, S. Moldovan, I. Janowska, W. Baaziz, R. Arenal, A. Wisnet, C. Scheu, S. Begin-Colin, D. Begin, C. Pham-Huu and O. Ersen, *Nature Comm.*, 2015, **5**, 4109.

28 Z. Liu, Y. Gong, W. Zhou, L. Ma, J. Yu, J. C. Idrobo, J. Jung, A. H. Macdonald, R. Vajtai, J. Lou and P. M. Ajayan, *Nature Comm.*, 2013, **4**, 2541.

29 D. B. Evans and R. D. Pehlke, *Trans. Metall. Soc. AIME*, 1964 **230**, 1651–1656.

30 D. B. Evans and R. D. Pehlke, *Trans. Metall. Soc. AIME*, 1964 **230**, 1657–1662.

31 M. S. Yaghmaee and G. Kaptay, *Materials Science Forum*, 2003, **414-415**, 491–496.

32 Y. Liu, X. Zou and B. I. Yakobson, *ACS Nano*, 2012, **6**, 7053–7058.

33 A. L. Gibb, N. Alem, J.-H. Chen, K. J. Erickson, J. Ciston, A. Gautam, M. Linck and A. Zettl, *J. Am. Chem. Soc.*, 2013, **135**, 6758–6761.

34 Y. Wang and Y. Ding, *Ann. Phys.*, 2014, **526**, 415–422.

35 R. Ma, Y. Bando, H. Zhu, T. Sato, C. Xu and D. Wu, *J. Am Chem. Soc.*, 2002, **124**, 7672–7673.

36 X. Blase, A. Rubio, S. G. Louie and M. L. Cohen, *EPL-Europhys Lett.*, 1994, **28**, 335–340.

37 Z. Zhou, J. Zhao, Z. Chen, X. Gao, B. W. T. Yang and P. von Ragué Schleyer, *J. Phys. Chem. B*, 2006, **110**, 13363–13369.

38 K. Nordlund, M. Ghaly, R. Averback, M. Caturla, T. D. de la Rubia and J. Tarus, *Phys. Rev. B*, 1998, **57**, 7556–7570.

39 K. Albe and W. Möller, *Comput. Mater. Sci*, 1998, **1-4**, 111–115.

40 A. Lubk, F. Röder, T. Niermann, C. Gatel, S. Joulie, F. Houdellier, C. Magen and M. J. Hytch, *Ultramicroscopy*, 2012, **115**, 78–87.